Transparent and High-Refractive Index Thermoplastic Polymer Glasses using Evaporative Ligand Exchange of Hybrid Particle Fillers

Zongyu Wang[†§], Zhao Lu[‡§], Clare Mahoney[‡∥], Jiajun Yan[†], Rachel Ferebee[‡⊥], Danli Luo[‡], Krzysztof Matyjaszewski[†], Michael R. Bockstaller[*‡]*

†Department of Chemistry, Carnegie Mellon University, 4400 Fifth Ave., Pittsburgh, PA 15213

‡Department of Materials Science and Engineering, Carnegie Mellon University, 5000 Forbes Ave., Pittsburgh, PA 15213

*) corresponding author: bockstaller@cmu.edu, km3b@andrew.cmu.edu

Abstract

The development of high refractive index glasses on the basis of commodity polymer thermoplastics presents an important requisite to the further advancement of technologies ranging from energy efficient lighting to cost efficient photonics. This contribution presents a novel particle dispersion strategy that enables the uniform dispersion of zinc oxide (ZnO) particles in poly(methyl methacrylate) (PMMA) matrix to facilitate hybrid glasses with inorganic content exceeding 25% by weight, optical transparency in excess of 0.8/mm and a refractive index greater than 1.64 in the visible wavelength range. The method is based on the application of evaporative ligand exchange to synthesize poly(styrene-*r*-acrylonitrile) (PSAN)-tethered zinc oxide (ZnO) particle fillers. Favorable filler-matrix interactions are shown to enable the synthesis of isomorphous blends with high molecular PMMA that exhibit improved thermomechanical stability as compared to the pristine PMMA matrix. The concurrent realization of high refractive index and optical transparency in polymer glasses by modification of a thermoplastic commodity polymer could present a viable alternative to expensive specialty polymers in applications where high costs or demands for thermomechanical stability and/or UV resistance prohibit the application of speciality polymer solutions.

KEYWORDS: Zinc oxide (ZnO), hybrid material, ligand exchange, refractive index, nanocomposite, transparency.

Introduction

Optically transparent polymers with high refractive index offer opportunities for advanced and innovative designs in applications ranging from sensing,[1] solid state lighting[2-3] and optics.[4] The development of chemical routes to realize transparent high refractive polymer materials has thus become an important objective in materials engineering. Two important routes to realize high refractive polymers are the strategic design of highly polarizable repeat units and the addition of high refractive fillers to polymer materials.[5-6] The inclusion of sulphur-, phosphorous- or halogen-containing polyaromatic groups into repeat and backbone structures has been shown to be a particularly effective means to realize high refractive properties.[7-10] Examples include polyimides or polycarbazole as well as organometallic polymers that have demonstrated to enable a refractive index $n > 1.7$.[11] However, the chemical attributes of highly polarizable repeat units also give rise to features that are undesirable or limiting in many applications. Examples include the reduction of photothermal stability due to the presence of aromatic groups, potential birefringence due to the increased persistence length of polymer backbones as well as environmental concerns (for example, associated with halogens).

An alternative route to enable high refractive index (n) in polymer glasses is the addition of high refractive index inorganic particle fillers to amorphous polymer matrices.[12] This 'nanocomposite' approach is fundamentally motivated by 'effective medium models' that predict the average refractive index of the composite to be a weighted average of the properties of the constituents – ideally without compromising any of the other desirable physicochemical properties of the polymer matrix.[13] Advantages of the 'nanocomposite approach' encompass the economic viability of constituent materials and the possibility of augmenting the properties of thermoplastics for which effective processing methods are readily available. The prospect of

broadening the range of applications for commodity and engineering plastics provides thus a major impetus for research in high refractive index composite materials.

A number of high refractive index semiconducting inorganic nanofillers, such as ZnS,[14] ZnO[15] and TiO_2,[5] have been studied as additives to increase the *n* of polymer matrices. ZnO is a wide bandgap semiconductor that exhibits a high refractive index ($n \sim 2.0$ at $\lambda = 630$ nm),[16] high chemical stability, low absorption in the visible range,[17] high catalytic activity, and effective antibacterial and bactericide properties.[18-20] ZnO also has shown to be an effective scavenger for several compounds (such as H_2S) that are detrimental to the stability and performance of optoelectronic devices. ZnO nanofillers have thus attracted particular interest in applications ranging from solar cells,[21-22] organic light-emitting diode (OLED),[23-24] UV-shielding materials,[25-26] to field-emission displays, and optical sensors.[27-28] However, while the concept of particle addition to enhance the refractive index of a polymer matrix is appealing, in reality challenges arise due to optical scattering of particle fillers. The scattering losses can be related to the scattering cross-section of particle fillers that depends approximately on the square of the particle domain volume and dielectric contrast ($C^{sca} \sim V_p^2(\varepsilon_m - \varepsilon_p)^2$, with ε_m and ε_p denoting the dielectric constant of embedding medium and particle filler, respectively). This translates into the need for uniform dispersion of filler particles in the matrix polymer (thus avoiding the formation of large aggregate structures).[29-30]

Unfortunately, the synthesis of uniform dispersions of particles in high molecular polymers presents a challenge because of the small contribution of entropy to the overall free energy of mixing in polymer/particle blends.[31] Recent approaches towards high refractive polymer composites based on one-component particle brush solids or resins circumvent this

difficulty.[32-35] However, while these methodologies are elegant and have shown to result in excellent combinations of refractive and transmission properties, the costs associated with the materials as well as generally soft mechanical properties limit the application of existing methods. The synthesis of optically transparent thermoplastic polymer hybrids with inorganic fraction large enough to enable a significant increase of the refractive index thus remains an elusive goal. One strategy to accomplish this goal is the modification of particle fillers with polymers that form miscible blends with the respective matrix polymer. The latter has shown to be particularly effective in stabilizing particle-in-polymer dispersions even at high inorganic volume fractions.[35-38] The tethering of polymers is typically accomplished by means of exchange reactions with (typically low MW) ligands (i.e. 'grafting-to'). Unfortunately, in the case of high refractive index fillers such as ZnO, the absence of functional groups with strong binding affinity renders ligand exchange reactions difficult.

Here we present a novel approach for the efficient ligand exchange of ZnO nanoparticles and their subsequent stable dispersion in poly(methyl methacrylate) (PMMA) – an amorphous polymer that is widely used in optical components. In this approach, a volatile ligand (octylamine, OA) is used to enable the synthesis of nano-sized ZnO particles. The ligand is exchanged under evaporative conditions with low molecular polymeric tethers that are chosen to form a miscible blend with the target matrix polymer. This second step enables the formation of a uniform dispersion of particle fillers with high inorganic loadings. For the particular example of poly(styrene-co-acrylonitrile) (PSAN) tethered ZnO, the approach is demonstrated to enable the synthesis of transparent poly(methyl methacrylate) (PMMA)/ZnO films with inorganic content exceeding 25 wt% and refractive index $n \sim 1.64$.

Experimental Section

Materials. Monomers: styrene (S, 99%, Aldrich), acrylonitrile (AN, 99%, Aldrich) were purified by passing through a column filled with basic alumina to remove the inhibitor. Tris(2-dimethylaminoethyl)amine (Me_6TREN, 99%, Alfa), zinc 2-ethylhexanoate ($Zn(EH)_2$, 80% in mineral spirits, Alfa), N-(2-hydroxyethyl)phthalimide (NHP, 99%, Acros), hydrochloric acid (HCl, 36.5-38.0%, Sigma), anisole (99%, Aldrich), methylene chloride (DCM, 99.5%, Fisher), tetrahydrofuran (THF, 99%, VWR), methanol (99%, VWR), hexane (99%, VWR), acetone (99%, VWR), N,N-dimethylformamide (DMF, 99%, VWR), α-bromoisobutyryl bromide (2-BiBB, Aldrich), ethyl 2-bromoisobutyrate (EBiB, 98%, Aldrich), copper(II) bromide ($CuBr_2$, 99%, Aldrich), triethylamine (TEA, 98%, Aldrich), diphenyl ether (DPE, 99%, Aldrich)， tin(II) 2-ethylhexanoate ($Sn(EH)_2$, 95%, Aldrich), poly(methyl methacrylate (PMMA, M_w = 120,000 by GPC, Aldrich) and octylamine (OA, 99%, Aldrich) were used as received without further purification.

Synthesis of PSAN capped ZnO nanoparticles. The three steps for the synthesis of PSAN capped ZnO NPs consist of a) the synthesis of OA-capped ZnO, b) the synthesis of PSAN-NH_2 ligands, and c) ligand exchange reaction between OA and polymer ligands. OA-capped ZnO NPs were synthesized as reported by Epifani and Weber.[38-39] The resulting product was dispersed in THF. A stock solution was prepared for use in further experiments. As shown in Scheme 1, NHP and TEA were reacted with 2-BiB in dry THF solution to form ATRP initiator. Low MW PSAN (M_n = 2300 with M_w/M_n = 1.13) with a protected NH_2 end group was synthesized via ARGET ATRP using 2-(phthalimido)ethyl 2-bromoisobutyrate with a protected amine functional group as an initiator, $CuBr_2$/Me_6TREN as catalytic complex and $Sn(EH)_2$ as reducing agent. The PSAN-NH_2

was obtained by the deprotection of NH_2 group with hydrazine. The ligand exchange reactions were conducted under N_2 atmosphere. OA-capped ZnO stock solution and polymer ligands were mixed in DPE to obtain a clear mixture at 220 °C for 2 h. The products were washed with cold hexanes. Three "selective precipitation, centrifugation, and dissolving" cycles were applied to completely remove the unattached polymer ligands.[40]

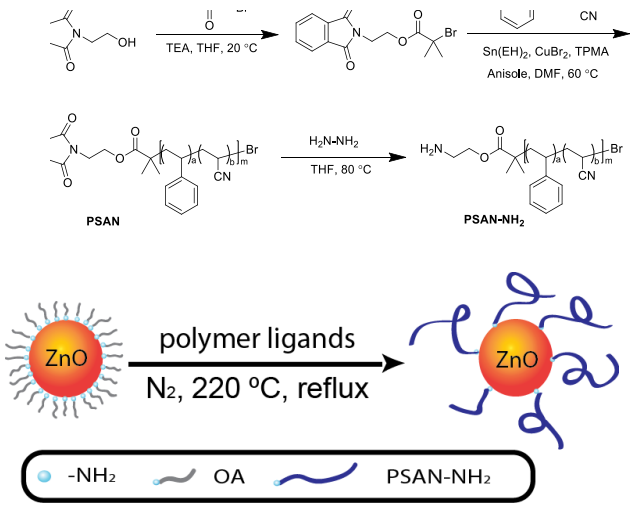

Scheme 1. Synthesis of PSAN-NH_2 polymer ligands and PSAN capped ZnO nanoparticles.

Fabrication of thin and bulk films of ZnO/PMMA hybrid materials. The PSAN capped ZnO NPs were dispersed in THF via sonication. The concentration was measured gravimetrically by air-drying 5 mL of the dispersion. Specific amounts of linear poly(methyl methacrylate) (PMMA, M_n = 120,000) powder and PSAN/OA-capped ZnO NPs dispersion were mixed in order to cast films with a series of different weight fraction of ZnO. After stirring for 24 h, 500 μL of the homogeneous dispersions were diluted with 10 mL THF. Thin films (<100 nm) were prepared by spin casting the diluted solution on silica wafer at the rate of 3000 rpm. The remaining bulk dispersions were transferred into 1.2-inch-diameter cylindrical Teflon molds. After slowly

evaporating solvent over 48 h at room temperature, transparent nanocomposite films of thickness ~ 0.5 mm formed. The residual solvent was removed from the bulk films by transferring it to a vacuum oven and slowly increasing the temperature at the rate of 10 ºC per 24 h to 150 ºC. Four specific bulk film compositions were investigated to systematically elucidate the effect of surface modification and the inorganic fraction on the thermo-mechanical and optical properties of nanocomposite films. The respective sample compositions and sample-IDs are summarized in Table 1.

Table 1. Compositions of pure PMMA and PMMA/PSAN capped ZnO bulk films

Sample ID	f_{ZnO}[a]	$f_{PSAN/OA}$[b]	f_{PMMA}[b]
Pure PMMA	0	0	100
OA-ZnO/PMMA	10	1.8	88.2
PSAN-ZnO/PMMA-1	10	6.7	83.3
PSAN-ZnO/PMMA-2	18	12	70.0
PSAN-ZnO/PMMA-3	27	18	55.0

a Determined by TGA; b calculated according to TGA data.

Characterization. Transmission electron microscopy (TEM) was carried out using a JEOL 2000 EX electron microscope operated at 200 kV. The average sizes of the ZnO NPs were determined from statistical analysis of the TEM micrographs using ImageJ software. Dynamic light scattering (DLS) using a Malvern Zetasizer Nano ZS was performed to confirm results obtained from TEM. It was also employed to determine volume-weighted average hydrodynamic diameters and distribution. A Philips X'Pert (Philips Analytical, Netherlands) X-ray

diffractometer (XRD) (Cu Kα radiation) was operated at 45 kV and 40 mA in grazing incidence mode to characterize the structure and crystallinity.

Thermogravimetric analysis (TGA) with TA Instruments 2950 was used to measure the fraction of ZnO in the hybrids. The data were analyzed with TA Universal Analysis. The TGA plots were normalized to the total weight after holding at 120 ºC.

$$\sigma_{\mathrm{TGA}} = \frac{(1-f_{\mathrm{ZnO}})N_{\mathrm{Av}}\,\rho_{\mathrm{ZnO}}\,d}{6\,f_{\mathrm{ZnO}}\,M} \qquad (1)$$

where f_{ZnO} is the ZnO fraction measured by TGA , N_{Av} is the Avogadro number, ϱ_{ZnO} is the density of ZnO NPs (5.6 g/cm^3), d is the average diameter of ZnO NPs (5 nm), M is the molar mass of the capping agent.

The glass transition temperature (T_g) of PSAN capped ZnO in PMMA matrix with different inorganic content were measured by differential scanning calorimetry (DSC) with TA Instrument QA-2000. The same procedure was run three times, each involving the following steps: 1) hold at 25 ºC for 5 min; 2) heat to 150 ºC at a rate of 10 ºC/min; 3) hold for 5 min; 4) cool down to 25 ºC. The DSC data were analyzed with TA Universal Analysis and the T_g was directly acquired.

The optical transmittance of bulk films was determined using a Varian 50 Bio UV-Vis Spectrophotometer over the wavelength range from 300 nm to 800 nm. To quantitatively compare the transparency of films with different thickness, the measured data were normalized to equal thickness using the described logarithmic relationship. In this study, the transmittance was normalized to 300 μm.

The refractive index of the thin films was measured using AutoEL-II Automatic Ellipsometer equipped with a helium-neon laser (λ = 632.8 nm). The angle of incidence was fixed at 70° and a two homogeneous layer film model (silica + nanocomposite) was utilized for the analysis. At least 5 different spots were measured for each film.

The mechanical properties (elastic modulus and hardness) of the bulk films were measured using MTS Nanoindenter XP with a nanoscopic diamond-based Berkovich tip. The indentations were performed at a displacement rate of 0.05 nm per second up to a maximum load at 2 μm depth. The maximum load indentation was held for 10 s followed by the elastic recovery of the material. 100 indentations were performed on each film.

Polymer ligands were characterized by GPC and NMR, the detailed information was included in Supporting Information.

Results and Discussion

Octylamine (OA) was chosen as ligand because of its appropriate boiling point of 175 ºC that prevents rapid evaporation during thermolysis of $Zn(EH)_2$. Figure 1a and 1b depict representative electron micrographs (TEM) of OA-capped ZnO, revealing a uniform particle size with average diameter $\langle d \rangle = 5.2 \pm 0.6$ nm.

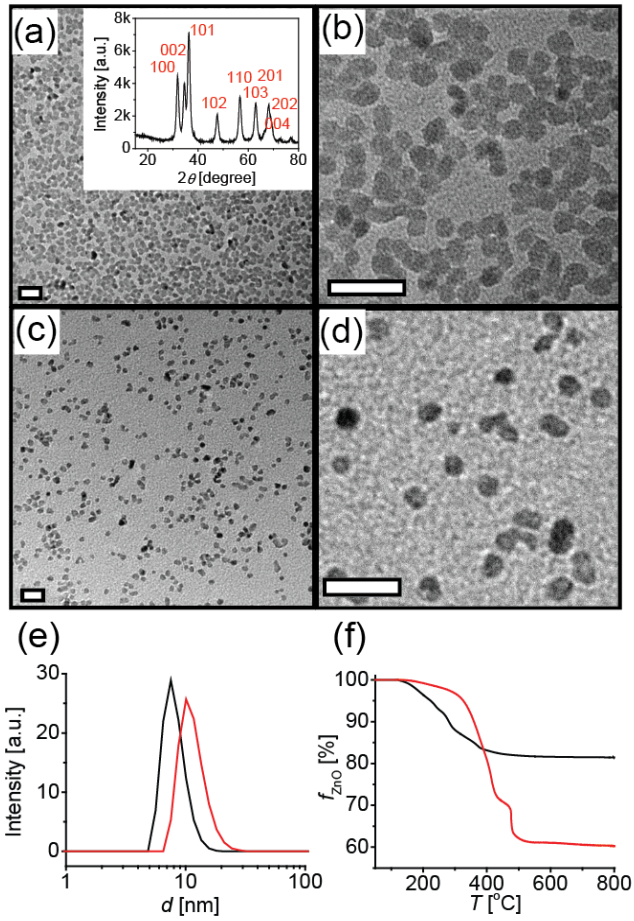

Figure 1. (a) and (b) TEM images of OA-capped 5 nm ZnO NPs, inset: XRD pattern of OA-capped ZnO; (c) and (d) TEM images of PSAN capped 5 nm ZnO NPs, M_n = 2300, M_w/M_n = 1.13; (e) Size distribution of OA/PSAN capped ZnO NPs measured by DLS in THF solution, intensity average particle size: OA-capped ZnO NPs, 7.5 nm, PSAN capped ZnO NP, 10.1 nm; (f) TGA traces of OA/PSAN capped ZnO NPs. Black line: OA-capped ZnO, red line: PSAN capped ZnO. Scale bars = 20 nm. Inset in Figure 1a depicts representative XRD pattern of OA-capped ZnO. Reflections correspond to the (100), (002), (101), (102) and (110) planes (PDF card nos: JCPDS-36-1451).

The typical particle yield of was 23%. X-ray diffraction analysis (see inset of Figure 1a) confirmed Wurtzite structure of ZnO. Dispersions of OA-capped ZnO NPs were stable in tetrahydrofuran (THF) or hexane for weeks, with negligible aggregation. Dynamic light scattering (DLS, Figure 1e) confirmed an intensity-average hydrodynamic size of about 7 nm in excellent agreement with TEM results. Thermogravimetric analysis revealed 83 wt% inorganic content (Figure 1f). From the inorganic content f_{ZnO} the ligand grafting density was determined to be 4.4 chains/nm^2. PSAN was selected as polymer tether for ligand exchange because PMMA/PSAN constitutes a miscible polymer blend with LCST behavior that shows reversible transition between miscible and phase separated states provided that the molar ratio χ = n(AN):n(S) is within the miscibility window $0.09 < \chi < 0.38$.[41] The interaction parameter of the PSAN/PMMA system depends on both the constitution of PSAN as well as the composition of the blend. In the present study, the molar composition of the random copolymer is S:AN = 3:1 – the corresponding interaction parameter is $\chi_{MMA/SAN} \approx -0.15$ (at $T \approx 25$ °C).

Ligand exchange of OA with PSAN-NH_2 was performed in DPE at T = 180 °C to concurrently drive the replacement reaction and extract unbound OA from the reaction mixture. The replacement reaction gave rise to a distinctive change in solubility characteristics. Whereas OA-capped ZnO NPs were stable in THF or hexane, PSAN-capped ZnO NPs after ligand exchange precipitated in hexane. Thus, free PSAN-NH_2 was removed by applying "selective precipitation, centrifugation, and dissolution" cycles.[40] As shown in Figure 1e, the DLS confirmed the ligand replacement by revealing an increase of the hydrodynamic diameter from 7.5 to 10.1 nm. Electron micrographs of the final ZnO-PSAN product (Figure 1c and 1d) further revealed negligible aggregation of particles after ligand exchange. The purified PSAN capped ZnO NPs

contain 60 wt% of ZnO (Figure 1f). Due to the large difference in steric hindrance, the grafting density of PSAN capped ZnO (0.7 chain/nm^2) was lower than OA-capped ZnO (4.4 chains/nm^2).

To understand the role of PSAN modification on particle/matrix interactions, we evaluated the thermomechanical properties of films as well as their microstructure. Figure 2 depicts heat flow curves of pristine and ZnO-PSAN filled PMMA revealing an increase of the glass transition temperature with particle filling content from T_g = 104 °C (for pristine PMMA) to T_g ~ 115 °C (for f_{ZnO} = 0.18). The increase of T_g supports previous reports on PMMA composites with PSAN-modified silica particle fillers and can be interpreted as a consequence of the attractive interactions between PSAN tethers and PMMA matrix.[31] Interestingly, the T_g of ZnO-PSAN/PMMA composites levels off at a ZnO filling fraction of f_{ZnO} ~ 0.18 (in fact a small reduction in T_g is observed for f_{ZnO} ~ 0.27). We rationalize this trend as a consequence of the large specific surface area of 5 nm ZnO fillers that implies the saturation of surface segment interactions at rather a low particle filling fractions. However, it should be noted that the effect of particle additives on T_g is a rather complex subject and alternative mechanisms could apply.[41-43]

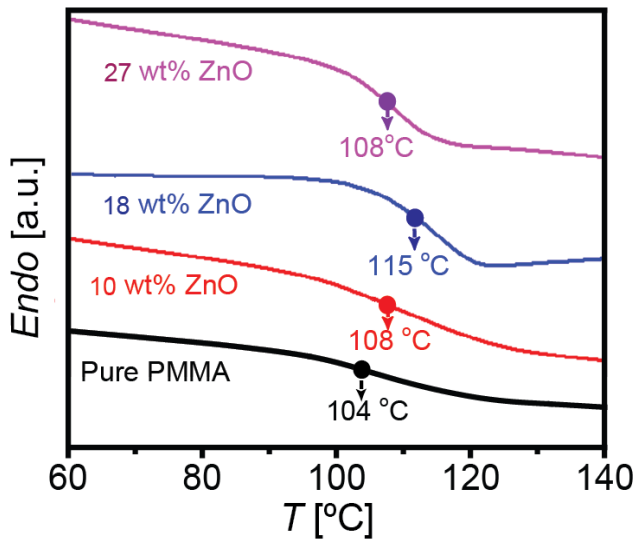

Figure 2. Heat flow curves of PSAN capped ZnO NPs system and corresponding PMMA reference polymer. The glass transition temperature(T_g) increased for PSAN capped ZnO materials.

The favorable interactions between ZnO-PSAN particle fillers and the PMMA matrix were confirmed by evaluation of the elastic modulus of composite films that was measured using nanoindentation of ~500 μm thick films. Figure 3 summarizes the elastic moduli and hardness values that were determined for the distinct ZnO-PSAN/PMMA systems.

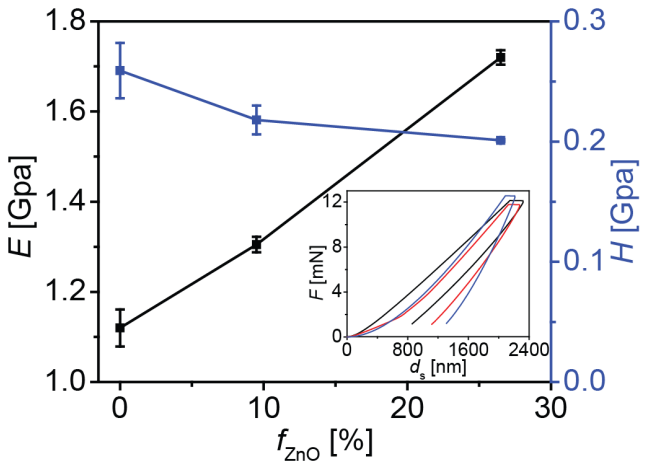

Figure 3. Nanoindentation measurement of PSAN capped ZnO in PMMA with different ZnO content indicate an increase of elastic modulus (E) and a small decrease of hardness (H) with increasing ZnO content; inset: Characteristic load (F)–displacement (d_s) curves for PSAN capped ZnO in PMMA with different ZnO content showing similar response: pure PMMA (black), 10 wt% ZnO (red), 27 wt% ZnO (blue).

The figure reveals an increase of the elastic modulus (E) from 1.12 GPa for pure PMMA to 1.31 GPa for 10 wt% PSAN capped ZnO and 1.72 GPa when the inorganic content was 27 wt%. Since the resistance to elastic deformation directly depends on the bonding strength in materials,

the 55% increase as compared to pristine PMMA provides clear support for increased dispersion interactions in the miscible PSAN/PMMA system. Here, a comment should be made regarding the application of nanoindentation to measure the elastic properties of polymer films. Nanoindentation was chosen primarily because of the ability to evaluate the mechanical properties of small material volumes. Because the mechanical characteristics are deduced from the interpretation of indent geometries rather than direct stress-strain measurements, the absolute values often differ from bulk values (sometimes by up to 20%).[44,45] However, trends have been shown to be correctly reproduced.

Characterization of the microstructure of PMMA/ZnO-PSAN composites by transmission electron microscopy (TEM) confirmed the randomly dispersed morphology, expected for miscible blends. Figure 4 depicts representative TEM images taken on micro-sections of bulk films of PMMA filled with PSAN and OA tethered ZnO particles at $f_{ZnO} \sim 0.1$.

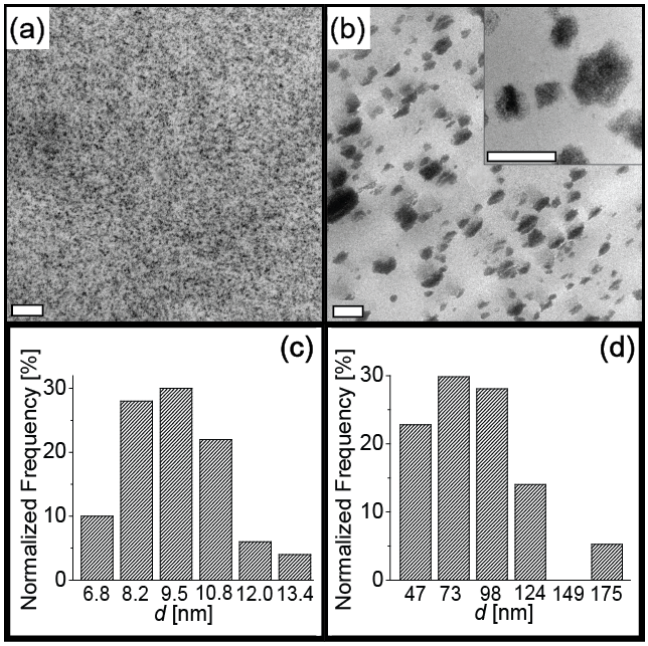

Figure 4. TEM images of ZnO/PMMA bulk films with 10 wt% ZnO contents (a) PSAN capped ZnO, (b) OA-capped ZnO, (c) and (d) size distributions of ZnO nanocomposite in the matrix, (c) PSAN capped ZnO, (d) OA-capped ZnO. Inset: higher magnification TEM images of OA-capped ZnO NPs in PMMA matrix. Scale bars are 200 nm.

Image analysis of micrographs such as Figure 4a reveals an average particle distance in the PMMA/ZnO-PSAN system (Figure 4a) is $\langle d_{p\text{-}p} \rangle$ = 1.1 nm, approximately equal to the expected particle distance of randomly dispersed structures $d_{th} = (V/N_p)^{1/3}$ = 0.9 nm (with N_p/V denoting the volume density of particles). A further indicator of a thermodynamically stable particle dispersion is the particle size distribution (Figure 4c) and the average particle diameter $\langle d \rangle$ = 10.1 nm (determined by image analysis) closely matches the value of the pristine ZnO-PSAN particles. This is in contrast to the microstructure observed in PMMA/ZnO-OA systems (Figure 4b) that reveals the formation of aggregates with an average size of $\langle d_{aggr} \rangle$ = 99.3 nm. The formation of aggregates is indicative of a phase separating system in which the balance of dynamics and thermodynamic driving forces determine the respective aggregate dimension. The different dispersion characteristics of ZnO-PSAN and ZnO-OA particle fillers have a profound impact on the optical properties of PMMA composite films. Figure 5 depicts photographs of films with systematic variation of ZnO content with and without PSAN modification. The figure reveals that optical transparency in ZnO-PSAN based composites (Figure 5b, 5c) is comparable to pristine PMMA (Figure 5a) while a significant loss of transparency is incurred upon dispersion of ZnO-OA particles in PMMA (Figure 5d) despite the significantly lower inorganic content. The opacity of ZnO-OA based composite films can be rationalized as a direct consequence of the aggregation behavior that is discerned from the micrograph shown in Figure 4b. In particular, the scattering cross-section of particle fillers depends on the square of the

particle volume and hence on the sixth power of the particle size (here it should be noted that in aggregating systems the term 'particle size' refers to the dimension of aggregate structures).[29-30] The clustering of ZnO particles observed in the immiscible PMMA/ZnO-OA system thus dramatically raises the scattering losses in phase-separating polymer/particle blend systems. ZnO containing particle films in Figure 5 exhibit a weak yellowish coloration. The latter is attributed to partial oxidation of excess amine ligands as well as to the preferential scattering of short wavelengths of small particle fillers (see below).

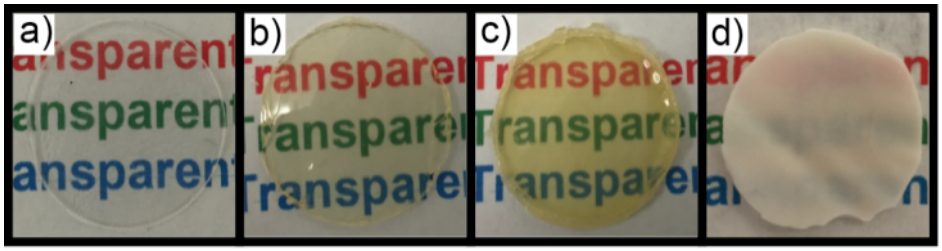

Figure 5. Photographs of pure PMMA, PSAN-capped ZnO/PMMA and OA-capped ZnO/PMMA hybrid bulk films: a) Pure PMMA (thickness: 666 μm); b) PSAN capped ZnO/PMMA-1 (10 wt% ZnO, 570 μm); c) PSAN capped ZnO/PMMA-2 (18 wt% ZnO, 646 μm); d) OA-capped ZnO/PMMA (10 wt% ZnO, 590 μm). The image area is 9 cm^2.

The transparency of the bulk films was quantitatively measured using UV-vis spectroscopy. Since each film had a different thickness, the measured data was normalized to equal film thickness as described in the experimental section. Figure 6 depicts the transmission curves (normalized to equal film thickness) for pristine PMMA and ZnO-PSAN/PMMA blend materials The figure reveals that optical transparency in excess of 0.8/mm^{-1} is retained for wavelengths $\lambda >$ 500 nm up to particle loadings of $f_{ZnO} = 0.18$.

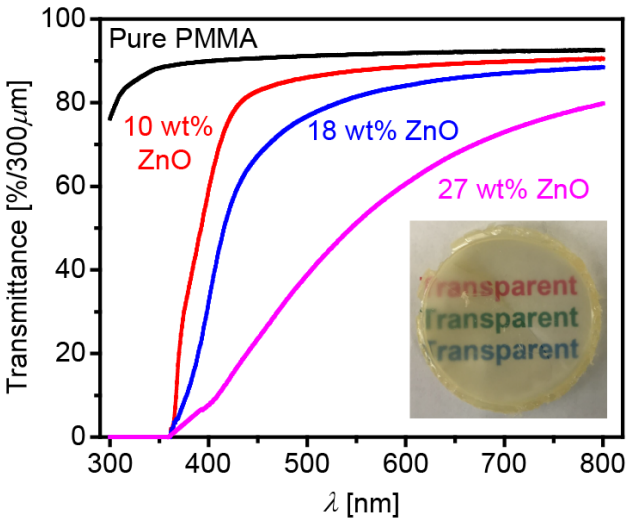

Figure 6. Normalized UV–vis transmittance spectra of the pure PMMA and the PSAN capped ZnO in PMMA matrix. The normalized transmittance corresponds to films with a thickness of 300 μm. Inset: photograph of PSAN capped ZnO/PMMA bulk films with 27 wt% ZnO (370 μm).

An optical transmission of 0.8 is commonly considered to be the threshold for a material to be recognized as 'transparent to the eye'.[46] All transmission curves shown in Figure 6 reveal a λ^{-y} dependence that is characteristic for scattering losses (in the limit of Rayleigh scattering $y = 4$). As expected, scattering losses increase with particle loadings, however, even at $f_{ZnO} = 0.27$ a transparency $T \sim 0.6\ (\text{length})^{-1}$ (at $\lambda = 500$ nm) is retained. For all systems, the transmittance vanished in the 300-365 nm range, due to UV absorption. This UV-blocking coincides with the absorption edge of 5 nm ZnO NPs that is estimated to be at 3.37 eV (or $\lambda = 369$ nm).[26,47] The high transparency in the visible range combined with a complete UV-cutoff could render PMMA/ZnO-PSAN composites interesting candidate materials for applications as transparent UV filters.

An intriguing application of low-scattering ZnO-particle fillers is in the fabrication of high refractive index polymer glasses that play an important role as optical materials. This is because ZnO exhibits a refractive index of n_{ZnO} = 1.973-2.105 in the visible range. Tethering of polymer chains alters the refractive index of particle fillers. The effective refractive index of ZnO-PSAN core-shell particles can be estimated using homogenization models such as Maxwell-Garnett (MG) theory as:

$$n_{\mathrm{eff,p}}{}^2 = n_{\mathrm{shell}}{}^2\left[1 + \frac{3\phi x}{1-\phi x}\right] \qquad (2)$$

where $x = (n_{core}^2 - n_{shell}^2)/(n_{core}^2 + 2\,n_{shell}^2)$; nshell and ncore represent the refractive index of the shell and core, respectively; and $\phi = v_{core}/(v_{core} + v_{shell})$ is the relative core volume. In this study, the n_{ZnO} and n_{PSAN} were assumed to be 1.989 and 1.558, corresponding to λ = 632 nm).[48] Using the compositional values as determined from TGA measurements, the effective refractive index of PSAN capped ZnO was calculated to be $n_{eff,p}$= 1.650. Note that the use of low MW polymer tethers is a critical prerequisite to enable high $n_{eff,p}$ of particle fillers since it facilitates a high inorganic content of the core-shell particles.

The effective refractive index of PMMA/ZnO-PSAN of composites formed with different concentrations of PSAN capped ZnO in a PMMA matrix was measured using ellipsometry at λ = 632 nm on thin film samples that were fabricated by spin coating of particle/polymer solutions (corresponding thick films could not be prepared due to the limited availability of particle systems). Figure 7a depicts the refractive index of composite films (red squares) as well as the trend predicted on the basis of effective medium theory (dotted line). The excellent agreement between experimental and theoretical values further supports the uniform distribution of particle fillers that is an assumption of the effective medium model. Note that due to the optical

dispersion characteristics of ZnO a higher refractive index is expected at a shorter wavelength (see inset of Figure 7a).

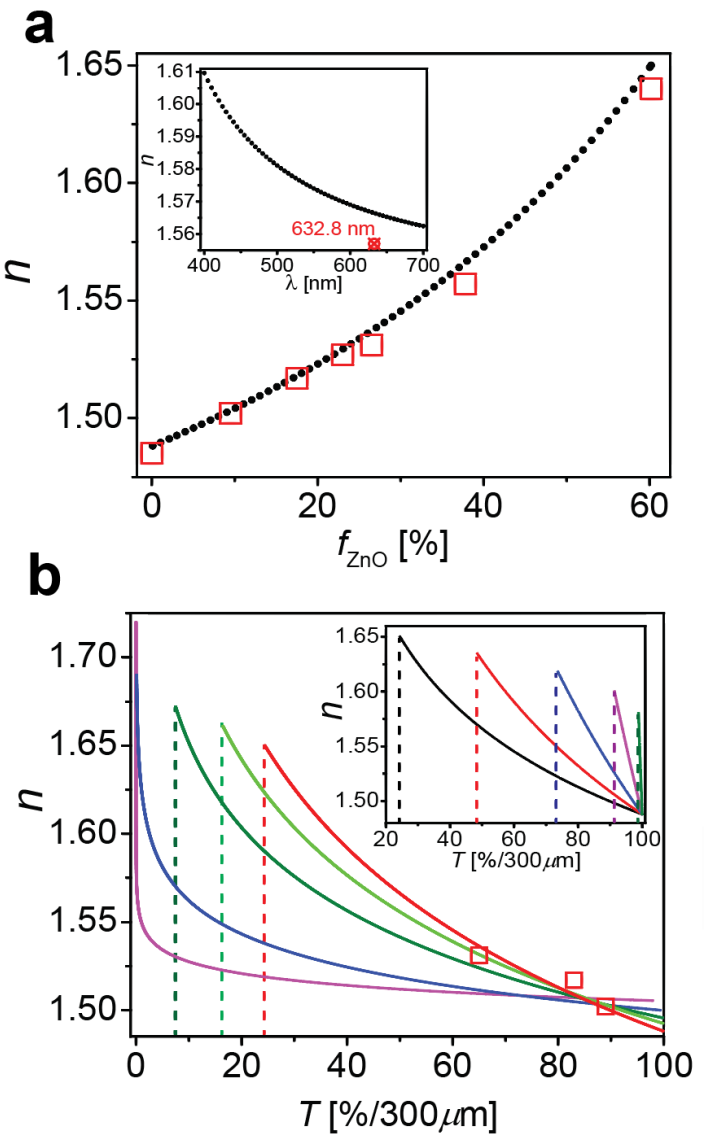

Figure 7. (a) Dependence of refractive index on ZnO content in hybrid thin films dashed line: theoretical trend line calculated using Maxwell Garnett theory; red squares: measured refractive index at 632.8 nm. Inset: refractive index of ZnO/PMMA hybrid bulk film (38 wt% ZnO contents) at a different wavelength. (b) Dependence of refractive index on the transmittance of hybrid films, theoretical trend line calculated using Beer-Lambert Law, red line: λ=633 nm,

green: 550 nm, olive: 500 nm, blue: 450 nm, magenta: 400 nm; red squares: measured refractive index at 633 nm. Inset: dependence of refractive index on transmittance of hybrid films at 633 nm with different size ZnO NPs, black line: 5nm, red: 4 nm, blue: 3 nm, magenta: 2 nm, green: 1 nm. Note that the maximum refractive index decreases with particle size due to the increased mass fraction of organic ligands.

To further evaluate the limitations of the nanocomposite approach a Mie scattering model was implemented to quantitatively relate the refractive and transmission properties of polymer films as a function of particle size (the details of the model are described in reference 30). The results of this simulation (see Figure 7b) reveal two important conclusions: First, the predicted scattering losses of the tested material systems are in excellent agreement with theoretical predictions (this justifies the application of Mie theory in the present case). Scattering losses increase with decreasing wavelength and hence the lower transmittances are observed at corresponding refractive index for shorter wavelengths (see main panel in Fig. 7b). Second, reducing the particle size is expected to significantly improve the optical figure of merit of films. Thus, whereas scattering losses result in the decrease of the transmission to $T \sim 0.2$ at a composition corresponding to the maximum refractive index ($n \sim 1.65$), the reduction of particle size to $d = 1$ nm is expected to enable $T \sim 0.95$ at $n \sim 1.6$ (here, a possible size dependence on the optical properties of ZnO has been neglected).

Conclusions

We have demonstrated a new method for the synthesis of optically transparent PMMA/ZnO hybrids with refractive index exceeding 1.6 in the visible range. The method rests on the

application of 'compatibilizing' polymer tethers (PSAN) that enable the stable dispersion of particles in the polymer host (PMMA) up to high inorganic loadings. PSAN capped 5 nm ZnO NPs were synthesized in high yield through evaporative ligand exchange. Particles were shown to be readily dispersible in PMMA up to weight fractions in excess of 35% resulting in films with high optical transparency (>0.8/mm) and refractive index exceeding 1.6 in the short wavelength visible range. Favorable filler/matrix interactions gave rise to concurrent enhancement of the mechanical properties (stiffness) of films. The observed increase of $n > 1.6$ presents a substantial increase in the refractive index of pristine PMMA that could promote its application in a range of optical applications. We note that this reported increase does not represent a fundamental limit in the achievable gain in the refractive index. Rather, a reduction in the degree of polymerization (or reduction of grafting density) of PSAN is expected to allow a further increase in the refractive index. Reduction of particle size is expected to enable a refractive index of ~1.6 at only minimal scattering losses. Optimization of these parameters is subject to our current research.

ASSOCIATED CONTENT

Supporting Information. GPC traces of polymer PSAN-NH_2 ligands, and TGA measurements of ZnO/PMMA bulk films. The Supporting Information is available free of charge on the ACS Publications website at

AUTHOR INFORMATION

Corresponding Author

* E-mail: bockstaller@cmu.edu (M.R.B.).

* E-mail: km3b@andrew.cmu.edu (K.M.).

Present Addresses

[Π] Materials and Manufacturing Directorate, Air Force Research Laboratory, 2941 Hobson Way, B654/R331Wright Pattern AFB, OH 45433-7750, USA.

[Δ] L'Oreal, 159 Terminal Ave, Clark, NJ, 07066, USA

Author Contributions

Z.W. synthesized materials, Z.L. performed character-ization work. J.Y. assisted in the synthesis; C.M., R. F., and D.L. assisted in the characterization work. M.R.B. and K.M. conceived and organized the project and together with Z.W. and Z.L. wrote the manuscript.

[§] Z.W. and Z.L. contributed equally to the work.

Notes

The authors declare no competing financial interest.

ACKNOWLEDGMENT

This work was supported by NSF (DMR 1501324 and DMR 1410845), the Department of Energy (DE-EE0006702), the National Science Center (grant UMO-2014/14/A/ST5/00204), as well as the Scott Institute for Energy Technologies at Carnegie Mellon University.

REFERENCES

(1) Maffli, L.; Rosset, S.; Ghilardi, M.; Carpi, F.; Shea, H. Ultrafast All-Polymer Electrically Tunable Silicone Lenses. *Adv. Funct. Mater.* **2015,** *25* (11), 1656-1665.
(2) Shen, T.-Z.; Hong, S.-H.; Song, J.-K. Electro-optical Switching of Graphene Oxide Liquid Crystals with an Extremely Large Kerr Coefficient. *Nat. Mater.* **2014,** *13* (4), 394-399.
(3) Schulz, H.; Mädler, L.; Pratsinis, S. E.; Burtscher, P.; Moszner, N. Transparent Nanocomposites of Radiopaque, Flame-Made Ta_2O_5/SiO_2 Particles in an Acrylic Matrix. *Adv. Funct. Mater.* **2005,** *15* (5), 830-837.
(4) Ucar, A. B.; Velev, O. D. Microfluidic Elastomer Composites with Switchable Vis-IR Transmittance. *Soft Matter* **2012,** *8* (44), 11232-11235.
(5) Lee, L.-H.; Chen, W.-C. High-Refractive-Index Thin Films Prepared from Trialkoxysilane-Capped Poly(methyl methacrylate)–Titania Materials. *Chemistry of Materials* **2001,** *13* (3), 1137-1142.
(6) Griebel, J. J.; Namnabat, S.; Kim, E. T.; Himmelhuber, R.; Moronta, D. H.; Chung, W. J.; Simmonds, A. G.; Kim, K.-J.; van der Laan, J.; Nguyen, N. A.; Dereniak, E. L.; Mackay, M. E.; Char, K.; Glass, R. S.; Norwood, R. A.; Pyun, J. New Infrared Transmitting Material via Inverse Vulcanization of Elemental Sulfur to Prepare High Refractive Index Polymers. *Adv. Mater.* **2014,** *26* (19), 3014-3018.
(7) Fan, Z.; Serrano, M. K.; Schaper, A.; Agarwal, S.; Greiner, A. Polymer/Nanoparticle Hybrid Materials of Precise Dimensions by Size-Exclusive Fishing of Metal Nanoparticles. *Adv. Mater.* **2015,** *27* (26), 3888-3893.
(8) Beecroft, L. L.; Ober, C. K. Nanocomposite Materials for Optical Applications. *Chem. Mater.* **1997,** *9* (6), 1302-1317.
(9) Janáky, C.; Rajeshwar, K. The Role of (Photo)Electrochemistry in the Rational Design of Hybrid Conducting Polymer/Semiconductor Assemblies: From Fundamental Concepts to Practical Applications. *Prog. Polym. Sci.* **2015,** *43*, 96-135.
(10) Barbey, R.; Lavanant, L.; Paripovic, D.; Schüwer, N.; Sugnaux, C.; Tugulu, S.; Klok, H.-A. Polymer Brushes via Surface-Initiated Controlled Radical Polymerization: Synthesis, Characterization, Properties, and Applications. *Chem. Rev.* **2009,** *109* (11), 5437-5527.
(11) Wei, Q.; Pötzsch, R.; Liu, X.; Komber, H.; Kiriy, A.; Voit, B.; Will, P.-A.; Lenk, S.; Reineke, S. Hyperbranched Polymers with High Transparency and Inherent High Refractive Index for Application in Organic Light-Emitting Diodes. *Adv. Funct. Mater.* **2016,** *26* (15), 2545-2553.
(12) Liu, J.-g.; Ueda, M. High Refractive Index Polymers: Fundamental Research and Practical Applications. *J. Mater. Chem.* **2009,** *19* (47), 8907-8919.
(13) Maldovan, M.; Bockstaller, M. R.; Thomas, E. L.; Carter, W. C. Validation of the Effective-medium Approximation for the Dielectric Permittivity of Oriented Nanoparticle-Filled Materials: Effective Permittivity for Dielectric Nanoparticles in Multilayer Photonic Composites. *Appl. Phys. B* **2003,** *76* (8), 877-884.
(14) Zhang, G.; Zhang, J.; Yang, B. Fabrication of Polymerizable ZnS Nanoparticles in N,N[prime or minute]-Dimethylacrylamide and the Resulting High Refractive Index Optical Materials. *Polym. Chem.* **2013,** *4* (14), 3963-3967.
(15) Demir, M. M.; Koynov, K.; Akbey, Ü.; Bubeck, C.; Park, I.; Lieberwirth, I.; Wegner, G. Optical Properties of Composites of PMMA and Surface-Modified Zincite Nanoparticles. *Macromolecules* **2007,** *40* (4), 1089-1100.

(16) Bond, W. L. Measurement of the Refractive Indices of Several Crystals. *Journal of Appl. Phys*. **1965,** *36* (5), 1674-1677.
(17) Khan, Z.; Khan, M.; Zulfequar, M.; Shahid Khan, M. Optical and Structural Properties of ZnO Thin Films Fabricated by Sol-Gel Method. *Mater. Sci. Appl*. **2011,** *2* (5), 340-345.
(18) Zhang, Z.-Y.; Xu, Y.-D.; Ma, Y.-Y.; Qiu, L.-L.; Wang, Y.; Kong, J.-L.; Xiong, H.-M. Biodegradable ZnO@polymer Core–Shell Nanocarriers: pH-Triggered Release of Doxorubicin In Vitro. *Angew. Chem. Int. Ed*. **2013,** *52* (15), 4127-4131.
(19) Xiong, H.-M. ZnO Nanoparticles Applied to Bioimaging and Drug Delivery. *Adv. Mater*. **2013,** *25* (37), 5329-5335.
(20) Noimark, S.; Weiner, J.; Noor, N.; Allan, E.; Williams, C. K.; Shaffer, M. S. P.; Parkin, I. P. Dual-Mechanism Antimicrobial Polymer–ZnO Nanoparticle and Crystal Violet-Encapsulated Silicone. *Adv. Funct. Mater*. **2015,** *25* (9), 1367-1373.
(21) Small, C. E.; Chen, S.; Subbiah, J.; Amb, C. M.; Tsang, S.-W.; Lai, T.-H.; Reynolds, J. R.; So, F. High-Efficiency Inverted Dithienogermole-Thienopyrrolodione-Based Polymer Solar Cells. *Nat. Photon*. **2012,** *6* (2), 115-120.
(22) You, J.; Dou, L.; Yoshimura, K.; Kato, T.; Ohya, K.; Moriarty, T.; Emery, K.; Chen, C.-C.; Gao, J.; Li, G.; Yang, Y. A Polymer Tandem Solar Cell with 10.6% Power Conversion Efficiency. *Nat. Commun*. **2013,** *4*, 1446.
(23) Yang, Q.; Liu, Y.; Pan, C.; Chen, J.; Wen, X.; Wang, Z. L. Largely Enhanced Efficiency in ZnO Nanowire/p-Polymer Hybridized Inorganic/Organic Ultraviolet Light-Emitting Diode by Piezo-Phototronic Effect. *Nano Lett*. **2013,** *13* (2), 607-613.
(24) Faria, J. C. D.; Campbell, A. J.; McLachlan, M. A. ZnO Nanorod Arrays as Electron Injection Layers for Efficient Organic Light Emitting Diodes. *Adv. Funct. Mater*. **2015,** *25* (29), 4657-4663.
(25) Huang, X.; Wang, X.; Wang, S.; Yang, J.; Zhong, L.; Pan, J. UV and Dark-Triggered Repetitive Release and Encapsulation of Benzophenone-3 from Biocompatible ZnO Nanoparticles Potential for Skin Protection. *Nanoscale* **2013,** *5* (12), 5596-5601.
(26) Zhang, Y.; Zhuang, S.; Xu, X.; Hu, J., Transparent and UV-Shielding ZnO@PMMA Nanocomposite Films. *Opt. Mater*. **2013,** *36* (2), 169-172.
(27) Xiong, M.; Gu, G.; You, B.; Wu, L. Preparation and Characterization of Poly(styrene butylacrylate) Latex/Nano-ZnO Nanocomposites. *J. Appl. Polym. Sci*. **2003,** *90* (7), 1923-1931.
(28) Lova, P.; Manfredi, G.; Boarino, L.; Comite, A.; Laus, M.; Patrini, M.; Marabelli, F.; Soci, C.; Comoretto, D. Polymer Distributed Bragg Reflectors for Vapor Sensing. *ACS Photonics* **2015,** *2* (4), 537-543.
(29) Bombalski, L.; Dong, H.; Listak, J.; Matyjaszewsk, K.; Bockstaller, M. R. Null-Scattering Hybrid Particles Using Controlled Radical Polymerization. *Adv. Mater*. **2007,** *19* (24), 4486-4490.
(30) Dang, A.; Ojha, S.; Hui, C. M.; Mahoney, C.; Matyjaszewski, K.; Bockstaller, M. R. High-Transparency Polymer Nanocomposites Enabled by Polymer-Graft Modification of Particle Fillers. *Langmuir* **2014,** *30* (48), 14434-14442.
(31) Ojha, S.; Dang, A.; Hui, C. M.; Mahoney, C.; Matyjaszewski, K.; Bockstaller, M. R. Strategies for the Synthesis of Thermoplastic Polymer Nanocomposite Materials with High Inorganic Filling Fraction. *Langmuir* **2013,** *29* (28), 8989-8996.
(32) Li, Y.; Wang, L.; Natarajan, B.; Tao, P.; Benicewicz, B. C.; Ullal, C.; Schadler, L. S. Bimodal "Matrix-Free" Polymer Nanocomposites. *RSC Adv*. **2015,** *5* (19), 14788-14795.

(33) Wong, M.; Guenther, J.; Sun, L.; Blümel, J.; Nishimura, R.; Sue, H.-J. Synthesis and Fabrication of Multifunctional Nanocomposites: Stable Dispersions of Nanoparticles Tethered with Short, Dense and Polydisperse Polymer Brushes in Poly(methyl methacrylate). *Adv. Funct. Mater.* **2012,** *22* (17), 3614-3624.
(34) Chung, P.-T.; Chiou, S.-H.; Tseng, C.-Y.; Chiang, A. S.-T. Preparation and Evaluation of a Zirconia/Oligosiloxane Nanocomposite for LED Encapsulation. *ACS Appl. Mater. & Interfaces* **2016,** *8* (15), 9986-9993.
(35) Braunecker, W. A.; Matyjaszewski, K. Controlled/Living Radical Polymerization: Features, Developments, and Perspectives. *Prog. Polym. Sci.* **2007,** *32* (1), 93-146.

(36) Hui, C. M.; Pietrasik, J.; Schmitt, M.; Mahoney, C.; Choi, J.; Bockstaller, M. R.; Matyjaszewski, K. Surface-Initiated Polymerization as an Enabling Tool for Multifunctional (Nano-)Engineered Hybrid Materials. *Chem. Mater.* **2014**, *26*, 745−762.
(37) Matyjaszewski, K.; Tsarevsky, N. V. Nanostructured Functional Materials Prepared by Atom Transfer Radical Polymerization. *Nat. Chem.* **2009,** *1* (4), 276-288.
(38) Epifani, M.; Arbiol, J.; Díaz, R.; Perálvarez, M. J.; Siciliano, P.; Morante, J. R. Synthesis of SnO2 and ZnO Colloidal Nanocrystals from the Decomposition of Tin(II) 2-Ethylhexanoate and Zinc(II) 2-Ethylhexanoate. *Chem. Mater.* **2005,** *17* (25), 6468-6472.
(39) Weber, D.; Botnaras, S.; Pham, D. V.; Steiger, J.; De Cola, L. Functionalized ZnO Nanoparticles for Thin-Film Transistors: Support of Ligand Removal by Non-thermal Methods. *J. Mater. Chem. C* **2013,** *1* (18), 3098-3103.
(40) Ehlert, S.; Taheri, S. M.; Pirner, D.; Drechsler, M.; Schmidt, H.-W.; Förster, S. Polymer Ligand Exchange to Control Stabilization and Compatibilization of Nanocrystals. *ACS Nano* **2014,** *8* (6), 6114-6122.
(41) Paul, D. R.; Barlow, J. W. A Binary Interaction Model for Miscibility of Copolymers in Blends. *Polymer* **1984,** *25* (4), 487-494.
(42) Moll, J.; Kumar, S. K. Glass Transitions in Highly Attractive Highly Filled Polymer Nanocomposites. *Macromolecules* **2012,** *45* (2), 1131-1135.
(43) Evans, C. M.; Sandoval, R. W.; Torkelson, J. M. Glass Transition Temperature of a Component near Infinite Dilution in Binary Polymer Blends: Determination via Fluorescence Spectroscopy. *Macromolecules* **2011,** *44* (17), 6645-6648.
(44) Choi, J.; Hui, C. M.; Pietrasik, J.; Dong, H.; Matyjaszewski, K.; Bockstaller, M. R. Toughening Fragile Matter: Mechanical Properties of Particle Solids Assembled From Polymer-Grafted Hybrid Particles Synthesized by ATRP. *Soft Matter* **2012,** *8* (15), 4072-4082.
(45) Oliver, W. C.; Pharr, G. M. Measurement of Hardness and Elastic Modulus by Instrumented Indentation: Advances in Understanding and Refinements to Methodology. *J. Mater. Res. Technol.* **2004,** *19* (01), 3-20.
(46) Narayanan, S.; Hajzus, J. R.; Treacy, C. E.; Bockstaller, M. R.; Porter, L. M. Polymer Embedded Silver-Nanowire Network Structures – A Platform for the Facile Fabrication of Flexible Transparent Conductors. *ECS J. Solid State Sci. Technol.* **2014,** *3* (11), P363-P369.
(47) Tang, E.; Cheng, G.; Pang, X.; Ma, X.; Xing, F. Synthesis of Nano-ZnO/Poly(methyl methacrylate) Composite Microsphere Through Emulsion Polymerization and Its UV-Shielding Property. *Colloid Polym. Sci.* **2005,** *284* (4), 422-428.
(48) Lee, Y.-J.; Ruby, D. S.; Peters, D. W.; McKenzie, B. B.; Hsu, J. W. P. ZnO Nanostructures as Efficient Antireflection Layers in Solar Cells. *Nano Lett.* **2008,** *8* (5), 1501-1505.

TOC GRAPHICS